Hindawi
International Journal of Energy Research
Volume 2024, Article ID 4550335, 11 pages
https://doi.org/10.1155/2024/4550335

Research Article

Displacement Mechanism and Flow Characteristics of Polymer Particle Dispersion System Based on Capillary Bundle Model

Yingfei Sui,[1] **Chuanzhi Cui**,[1] **Yidan Wang**,[2] **Shuiqingshan Lu**,[1] **and Yin Qian**[1]

[1]*National Key Laboratory of Deep Oil and Gas, China University of Petroleum (East China), Qingdao 266580, China*
[2]*West-to-East Gas Pipeline Company, National Petroleum and Natural Gas Pipe Network Group Co. Ltd., Shanghai 200122, China*

Correspondence should be addressed to Chuanzhi Cui; ccz2008@126.com

Received 28 December 2023; Revised 30 March 2024; Accepted 17 April 2024; Published 3 May 2024

Academic Editor: Abdallah Bouabidi

During the development of oil reservoirs, a rapid increase in water cut following reservoir flooding leads to inefficient or ineffective circulation of injected water, rendering a significant portion of the remaining oil in the reservoir inaccessible. The displacement method using polymer particle dispersion systems effectively solves the issue of rapid water breakthrough in oil reservoirs. Owing to the particle phase separation phenomenon, polymer particles can selectively penetrate into the larger pores where water circulation is inefficient, enhance their flow resistance, and thereby achieve equilibrium displacement along with an increased swept volume. This paper investigates the heterogeneous distribution of polymer particles within a porous medium, incorporates the red blood cell dendrite concentration distribution theory from biological fluid mechanics, and develops a mathematical model to delineate the viscosity characteristics of polymer particle dispersion systems, taking into account the phase separation phenomenon. Building on this foundation, it formulates a capillary bundle model for the polymer particle dispersion system specifically designed for oil displacement and proceeds to determine its relative permeability curve. Simulation outcomes reveal that at a water saturation level of 0.063, the concentration of polymer particles in fractured large pore capillaries is markedly elevated, yet capillaries with a pore size under 26 μm remain devoid of polymer particles. With the increase of water saturation, the concentration of polymer particles in large pore capillaries reduces, whereas it progressively augments in medium pore capillaries. Upon reaching a peak water saturation of 0.751, capillaries smaller than 18 μm are entirely free of polymer particles. These findings suggest that the heterogeneous distribution of polymer particles markedly inhibits the percolation capabilities of the dispersed system following a water phase breakthrough, facilitating the entry of more dispersion into oil-laden capillaries and thus enhancing the flow capacity of the oil phase.

1. Introduction

During the development of oil reservoirs, the effectiveness of water flooding is primarily hindered by variations in fluid mobility and an increased water cut. Water injection frequently flows through channels of high permeability, which significantly escalates the water cut. Consequently, water control has emerged as a critical and challenging aspect of water flooding operations. Polymer particles are capable of decreasing the flow velocity within channels of high permeability. By fine-tuning the injection parameters and the properties of the particles, the dispersion system being injected can selectively target pores from large to medium scale, diminishing the permeability of larger pores without impacting that of smaller ones. As a result, the flow velocity distribution, influenced by the heterogeneity of the reservoir, can be significantly ameliorated, thereby increasing the swept volume [1–4].

Current research on the oil displacement mechanisms of polymer particle dispersion systems primarily focuses on studying the hydration swelling characteristics of polymer particles, assessing plugging performance through experiments, and simulating macroscopic permeability laws via physical experiments [5–7]. The prevailing percolation theories largely draw upon traditional percolation theories and component models applicable to chemical flooding [8–10]. Numerous scholars have embarked on studies related to polymer particle flooding, yielding significant findings. Liu

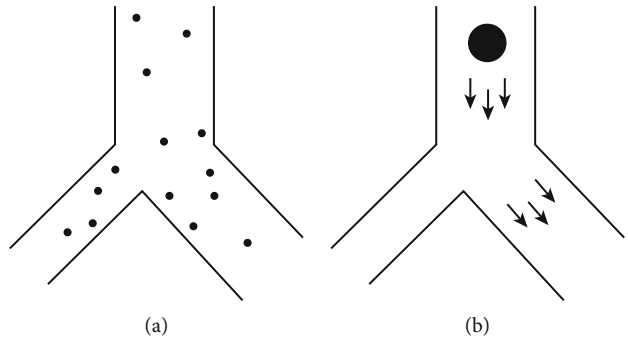

Figure 1: Schematic diagram of particle phase separation at automatically, where (a) is the uniform distribution of polymer particles and (b) is the heterogeneous distribution of polymer particles.

et al. [11] proposed a novel dual-dispersed profile control and displacement system (DDS), employing polymers and microspheres to obstruct polymer crossflow and enhance oil recovery. And the sealing efficacy of the DDS system was appraised via core displacement experiments. Luo et al. [12] assessed the effectiveness of innovative polymer-encapsulated silica nanoparticles (CM-NPs) as reservoir plugging materials in diminishing water content within multistage hydraulic fractured tight carbonate oil formations, utilizing core displacement experiments for evaluation. Sun et al. [13] employed microfluidic technology to mimic the particle phase separation phenomenon observed in SMG water dispersions during pore migration. Through physical simulation experiments, it was discovered that SMG particles and their carrier fluid act independently but collaboratively to mobilize residual oil in areas of relatively low permeability, thereby enhancing oil recovery.

The majority of numerical simulations and theoretical analyses addressing the flow dynamics of dispersion systems continue to employ methods and models designed for homogeneous solutions, overlooking the significant heterogeneity of dispersed systems and its consequential effects on flow behaviour. In liquid-solid two-phase dispersion systems like suspensions, the microstructure of the particle phase undergoes changes owing to the insolubility of solids in liquids, which in turn, influences the rheological properties of the system. Utilizing the capillary bundle model, this paper integrates the water absorption and swelling attributes alongside the viscoelastic properties of polymer particles, taking into account the heterogeneous percolation features of polymer particle dispersion systems and establishes a simulation approach for displacement, whereby the relative permeability curves for the oil and water phases are determined. The model proposed herein is particularly suitable for elucidating the percolation behaviour of nano/micron-scale polymer particles. Polymer particles, which expand to nearly millimetre-scale radii upon water absorption, can induce blockages in porous media, rendering this model inapplicable in such scenarios.

2. Flow Characteristics of Polymer Particle Dispersed Systems

2.1. Heterogeneous Distribution Phenomenon of Polymer Particles. The polymer particle dispersion system, comprising polymer particles and carrier fluids, forms a dispersed phase aimed at oil displacement. Unlike polymer solutions, these systems exhibit a nonuniform spatial distribution of polymer particles during flowing, leading to phase separation, where particle concentrations vary within the porous medium's branched channels. Experimental evidence [14] has shown that polymer particles fail to penetrate $2\,\mu$m microtubes and move slowly through $5\,\mu$m microtubes, whereas in $10\,\mu$m microtubes, the movement of polymer microsphere solutions is notably quicker. Further, nuclear magnetic resonance studies by Zhou et al. [15] have revealed that micron-sized polymer particles predominantly infiltrate pores larger than $20\,\mu$m during oil flooding and also initiate oil recovery in pores ranging from 8 to $500\,\mu$m. These researches collectively underscore the phase separation and heterogeneous distribution of polymer particles in the oil recovery process of polymer particle dispersion systems.

Existing experimental and theoretical studies [16–18] have revealed that the phase separation observed in dispersed systems stems from microstructural changes in the particle phase, induced by shear forces during flow. Once polymer particles undergo hydration and expansion, they absorb water, becoming easily deformable and moving towards the channel's axis under shear stress. Figure 1 presents a schematic of a porous medium, illustrating fluid entry from the top and exit through two outlets at the bottom. In Figure 1(a), particle sizes below $1\,\mu$m result in Brownian motion predominance, with particle concentration evenly distributed between both outlets due to diffusion. Conversely, as depicted in Figure 1(b), particles exceeding $1\,\mu$m in size, upon expansion, are centralized within the channel by fluid shear forces. This leads to a preferential selection of the exit offering less resistance and higher flow velocity, causing a reduced particle phase presence and diminished concentration in the microchannels of the exit with lower velocity.

2.2. Mathematical Model of Heterogeneous Distribution of Polymer Particles. The study of phase separation has attracted considerable interest in biofluid mechanics, highlighted by microfluidic experiments on blood flow. These experiments have shown that, in bifurcations with notably different diameters, a reduced number of red blood cells migrate into the narrower branch. This observation

underlines the heterogeneous distribution of particle phases within the branching channels. Drawing parallels between the dynamics of polymer particles in porous media and red blood cells' circulation, we adopt and adapt the concept of dendritic branching concentration distribution from biofluid mechanics. This approach is used to develop a mathematical model that accurately represents the heterogeneous concentration distribution of polymer particles across pores of varying dimensions.

Assuming there are N capillaries and the flow rate of each capillary is represented as

$$f_i = \frac{q_i}{\sum_{i=1}^{N} q_i}, \quad i = 1.\cdots N, \tag{1}$$

where q_i represents the flow rate of the i-th capillary.

The average volume concentration of the particles after hydration and expansion can be expressed as a function of the expansion ratio:

$$\phi_0 = \phi_{\text{ini}}(1 + \text{SR})^3, \tag{2}$$

where φ_{ini} is the volume concentration before expansion and SR is the expansion ratio.

The definition of the volume concentration component within each capillary is given by

$$\theta_i = \frac{\phi_i}{\phi_0}, \tag{3}$$

where φ_i is the particle volume concentration of the i-th capillary.

Based on the conservation laws of fluid mass and particle mass, we can derive

$$\begin{aligned} \sum_{i=1}^{N} f_i &= 1, \\ \sum_{i=1}^{N} f_i \theta_i &= 1. \end{aligned} \tag{4}$$

Introducing and modifying the expression for the concentration component of red blood cells in a tree-like bifurcation [19, 20], we obtain the volume concentration component equation for any N capillaries of polymer particles:

$$\begin{aligned} \bar{f}_i &= f_i \times \frac{N}{2}, \quad i = 1.\cdots N, \\ \theta_i(f_i) &= a + \frac{1\text{-}a}{2\bar{f}_i}, \quad i = 1.\cdots N. \end{aligned} \tag{5}$$

The branch flow f_i with particle concentration component θ_i equals to 0 is defined as the critical branch flow f_i^*. According to the above calculation, when the capillary branch flow f_i is less than the critical branch flow f_i^*, $\theta_i < 0$, so the equation is further revised. A new parameter fs is introduced, and the following equations for the volume concentration component of polymer particles in any N capillaries are obtained:

$$\theta_i(f_i) = a + \frac{1\text{-}f_s a}{2f_i}, \quad f_i > f_i^*, \tag{6}$$

$$\theta_i(f_i) = 0, \quad f_i < f_i^*, \tag{7}$$

$$\bar{f}_i = f_i \times \frac{N^*}{2}, \tag{8}$$

where f_s is the sum of the flow rates for all capillaries with $f_i > f_i^*$ and $N*$ is the number of capillaries with $f_i > f_i^*$.

This improved model satisfies the conservation of particle mass and effectively simulates the phenomenon of phase separation.

According to the Krige-Dougherty equation [21] for viscosity, the viscosity expression for the polymer particle dispersion system can be obtained as follows:

$$\eta = \eta_s \left(1 - \frac{\phi_i}{\phi_m}\right)^{-B\phi_m}, \tag{9}$$

where η_s is the viscosity of the solvent, B is the Einstein constant, φ_i is the volume concentration of particles in the i-th capillary, and φ_m is the maximum volume concentration of solid particles.

In Equation (9), B and φ_m are parameters that need to be fitted with experimental data. According to the viscosity expression in Equation (9) and the particle concentration component θ_i in each capillary and the average volume concentrationφ_0 of the particles after hydration expansion, the viscosity of the displacement fluid in each capillary can be obtained.

The phenomenon of particle phase separation leads to variations in particle volume concentration across different capillaries, thereby affecting the viscosity of the displacement fluid uniquely in each capillary. A higher flow rate within a capillary correlates with a greater concentration of particles and, consequently, a higher viscosity of the displacement fluid. This increase in viscosity enhances the flow resistance in larger capillaries, favorably impacting the extraction of residual oil from smaller capillaries.

3. Consider the Mathematical Model of Capillary Bundle Oil Displacement with Heterogeneous Distribution of Polymer Particles

3.1. Uniform Phase Displacement Oil Capillary Bundle Model considering Boundary Layer Effects. During the oil displacement process, if polymer particles are distributed uniformly, their concentration remains consistent across all pores, resulting in a stable viscosity for the dispersion system. This condition mirrors the displacement characteristics observed with a polymer solution, thus allowing the homogeneous dispersion system to be analogized to a polymer solution.

Several techniques exist for determining the relative permeability of oil and water [22, 23]. This study utilizes the JBN method [24] for its solution approach. By leveraging the foundational capillary bundle model and accounting for the boundary layer effect, a mathematical model specifically for oil displacement in capillary bundles has been formulated.

Considering the two-phase flow process of polymer solution displacement oil in the capillary, the pressure difference at both ends is Δp. Assuming that the capillary is filled with oil phase and is oil-wet, there is an immobile oil film on the capillary wall, that is, a boundary layer, forming residual oil. According to the Poiseuille theorem, the flow rate expression of two-phase laminar flow in the capillary can be obtained as shown in

$$q = \frac{\pi(r-\delta)^4}{8}\left[\frac{\Delta p + p_c}{\mu_w x + \mu_o(L-x)}\right], \tag{10}$$

where r is the capillary radius in meters (m), p_c is the capillary pressure in pascal (Pa), δ is the boundary layer thickness in meters (m), μ_w is the viscosity of polymer solution (mPa·s), μ_o is the viscosity of oil phase (mPa·s), x is the position of the oil-water interface in meters (m), and L is the length of the capillary in meters (m).

The boundary layer thickness is a function related to the capillary radius and can be expressed as follows [25, 26]:

$$\delta = r \cdot a \cdot e^{b \cdot r}(\nabla p)^c \cdot \mu_o, \tag{11}$$

where a, b, and c are parameters that need to be fitted based on experimental data.

The flow rate can be expressed as

$$q = \pi(r-\delta)^2 \frac{dx}{dr}. \tag{12}$$

Equations (12) and (13) describe the first-order differential equation that represents the variation of the oil-water interface position with time t:

$$\frac{dx}{dt} = \frac{(r-\delta)^2}{8}\left[\frac{\Delta p + p_c}{\mu_w x + \mu_o(L-x)}\right]. \tag{13}$$

The initial conditions are

$$t = 0, \tag{14}$$

$$x(t) = L_0. \tag{15}$$

Solving this ordinary differential equation yields the position of the oil-water interface at any given time t:

$$x(t) = -\frac{\mu_o L}{\mu_w - \mu_o} \pm \frac{1}{2}\sqrt{4L^2\left(\frac{\mu_o}{\mu_w - \mu_o}\right)^2 + \frac{(r-\delta)^2}{\mu_w - \mu_o}(\Delta p + p_c)t + 4L_0{}^2 + \frac{8LL_0\mu_o}{\mu_w - \mu_o}}. \tag{16}$$

When the viscosity of the polymer solution is greater than the viscosity of the oil phase, the positive square root is taken; when the viscosity of the polymer solution is less than the viscosity of the oil phase, the negative square root is taken.

For the initial moment $t = 0$, Equation (16) simplifies to

$$x(t) = -\frac{\mu_o L}{\mu_w - \mu_o} \pm \frac{1}{2}\sqrt{4L^2\left(\frac{\mu_o}{\mu_w - \mu_o}\right)^2 + \frac{(r-\delta)^2}{\mu_w - \mu_o}(\Delta p + p_c)t}. \tag{17}$$

Equations (13) and (14) can be used to calculate the time for the displacement fluid to reach the outlet from the initial position:

$$t = \left(\frac{m-1}{2}\left(L^2 - L_0{}^2\right) + L(L - L_0)\right)\frac{8\mu_o}{(r-\delta)^2(\Delta p + p_c)}, \tag{18}$$

where m is the ratio of the viscosity of the water phase to the viscosity of the oil phase.

Taking the derivative of Equation (16) with respect to time, the flow rate expression for the oil-water interface at any position in the capillary is given as follows:

$$q_o = \pi\frac{(r-\delta)^4(\Delta p + p_c)}{8\sqrt{(\mu_o L)^2 - (\mu_o - \mu_w)\left[\left(\left((r-\delta)^2 t\right)/4\right)(\Delta p + p_c) + 2\mu_o LL_0 - L_0{}^2(\mu_o - \mu_w)\right]}}. \tag{19}$$

When the water phase breakthrough occurs in the capillary, the flow rate is described by the Poiseuille equation as follows:

$$q_w = \frac{\pi(r-\delta)^4}{8\mu_w}\frac{\Delta p}{L}. \tag{20}$$

Assuming the minimum radius of the capillary where water breakthrough occurs is r_{bt}, the oil-water flow rate at the outlet can be expressed as follows:

$$Q_w = \int_{r_{bt}}^{r_{\max}} q_w df(r), \tag{21}$$

$$Q_o = \int_{r_{\min}}^{r_{bt}} q_o df(r), \tag{22}$$

where $f(r)$ represents the probability density function corresponding to different capillary radius.

The water saturation at the outlet of the capillary bundle, $S_{w\,\mathrm{out}}$, at any given time is calculated as follows:

$$S_{w\,\mathrm{out}} = \frac{\int_{r_{bt}}^{r_{\max}}\left(r_p - \delta\right)^2 df(r)}{\int_{r_{\min}}^{r_{\max}} r^2 df(r)}. \tag{23}$$

According to the Darcy flow equation of oil-water two-phase, it can be obtained as follows:

$$Q_w = \frac{K_{rw}KA}{\mu_w}\frac{\Delta p}{L_b}, \tag{24}$$

$$Q_w = \frac{K_{rw} K A}{\mu_w} \frac{\Delta p}{L_b}. \quad (25)$$

L_b is the apparent length of the core shown by the capillary bundle, and its expression is shown as follows:

$$L_b = \frac{L}{\tau}. \quad (26)$$

τ is the tortuosity, which is a constant related to porosity, and its expression is

$$\tau = 0.8 \cdot (1 - \text{poro}) + 1. \quad (27)$$

The absolute permeability and the relative permeability of the oil-water two-phase at any time of the capillary bundle model can be calculated by Equations (21) and (22) and Equations (24) and (25). The solution idea is shown in Figure 2.

3.2. Capillary Bundle Model for Oil Displacement considering Heterogeneous Distribution of Polymer Particles. With constant pressure applied at both ends, a capillary's breakthrough results in reduced resistance, altering the flow rates across all capillaries. Experiments show that the polymer particle dispersion system prefers pathways of low resistance and high velocity. Thus, following a capillary breakthrough, recalculating the flow rates, polymer particle concentrations, and viscosities within each capillary becomes imperative. This recalibration often results in heightened polymer particle concentration within the breakthrough capillary, subsequently increasing its flow resistance.

Due to the change in viscosity of the injected dispersion system, the fluid breakthrough time in each capillary is recalculated based on Equation (18). The smallest breakthrough time is chosen as the iteration step, and then, the variation of the oil-water interface position in each capillary is calculated using Equation (17). The outlet flow rate and water saturation values are determined using Equations (18)–(23), while the relative permeability values of the two phases are calculated using Equations (24) and (25). This process is repeated until there is no oil phase flow. The solution approach is illustrated in Figure 3.

4. Results and Discussion

Assuming the throat radius of the capillaries follows a Rayleigh distribution, its probability density function is expressed as

$$f(r) = \frac{r}{\sigma^2} \exp\left(-\frac{r^2}{2\sigma^2}\right), \quad (28)$$

where σ is the Rayleigh distribution parameter, and in this paper, it takes a value of 1.596.

Assuming a total of 1000 capillaries with radii distributed from 1 μm to 55 μm (Figure 4), all capillaries are oil wet. According to the Rayleigh distribution, the calculated absolute permeability of the capillary model is 170.9 mD (K). The porosity (φ) is set to 0.33, and based on Equation (27), the tortuosity (τ) is calculated as 1.536.

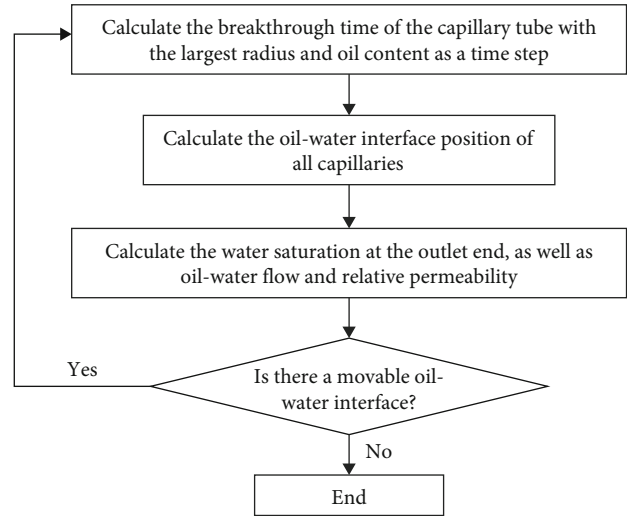

Figure 2: The solution approach for the capillary bundle model with uniform distribution of polymer particle.

The simulation parameters are as follows: the initial particle size of the polymer particles is 2 μm, the expansion factor (SR) is 1, the separation coefficient a in Equation (6) is set to 2, the interfacial tension is 0.02 N/m, the contact angle is 120 degrees, and the initial particle concentration is 0.008. The displacement is carried out under constant pressure conditions with a displacement pressure of Δp equals 1 MPa. The solvent of the dispersion system is water, and the viscosity of water is 1 mPa·s, and the viscosity of oil is 10 mPa·s.

4.1. Capillary Bundle Model for Oil Displacement considering Heterogeneous Distribution of Polymer Particles. According to the boundary layer thickness expression (Equation (11)), the corresponding boundary layer thickness of each capillary can be obtained. In the equation, the values of a, b, and c are 0.25763, -0.261, and -0.419, respectively.

Utilizing the mathematical model and parameters previously defined, Figure 5 presents the simulation outcomes for both the uniform phase and the polymer particle dispersion systems. In this context, the uniform phase displacement refers to the solvent (water) movement through the dispersion system. Corresponding results from the laboratory core displacement experiments are depicted in Figure 6 [20].

The capillary bundle model developed in this study exhibits an absolute permeability of 170.9 mD, whereas the absolute permeability recorded in laboratory core displacement experiments stands at 105.9 mD, indicating that the model's parameters are in a reasonable agreement with experimental data.

As showed in Figure 5, the peak water saturation (Sw) reaches 0.751 due to the boundary layer effect. Given that each capillary is oil-wet, the oil phase within the boundary layer remains immobile against the displacing water phase, leading to the presence of unusable residual oil. Consequently, the saturation level of the water phase cannot achieve 1. A comparison between Figures 5 and 6

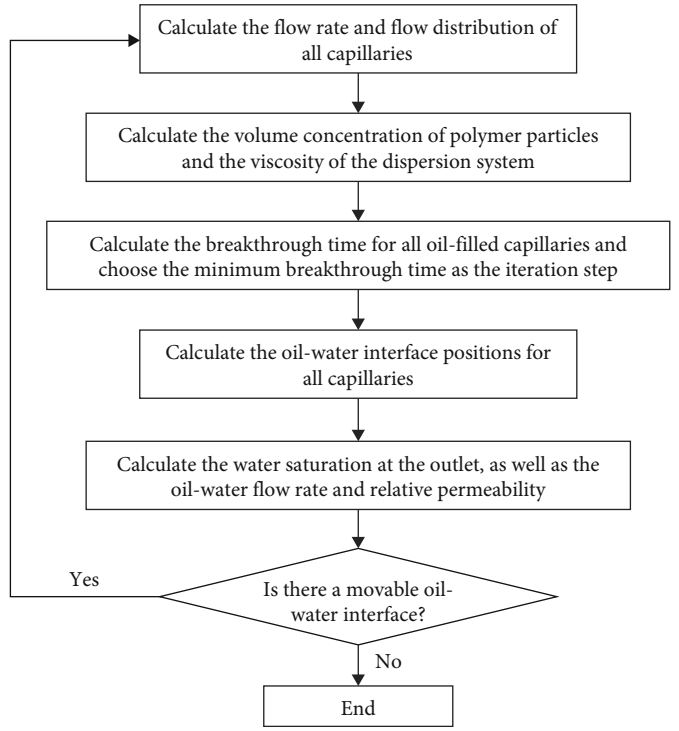

Figure 3: The solution approach for the capillary bundle model with heterogeneous distribution of polymer particles.

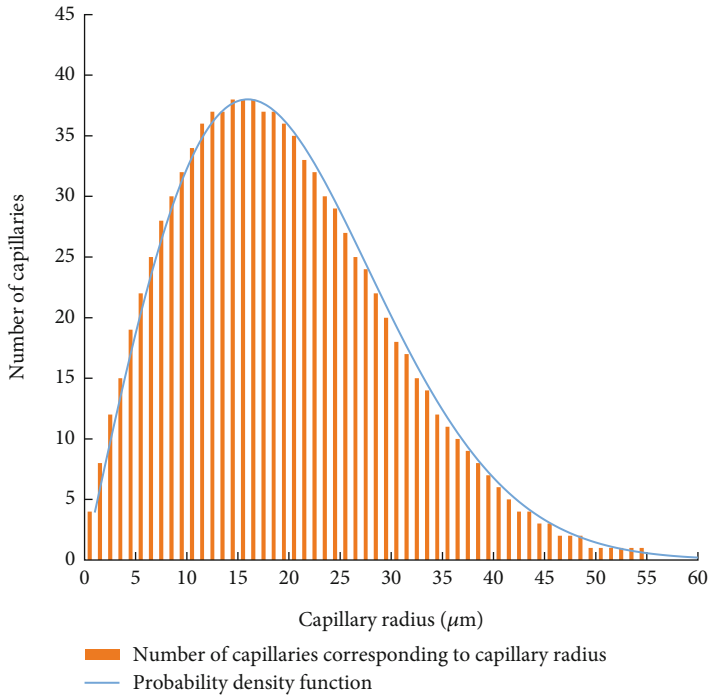

Figure 4: The number of capillaries corresponding to different capillary radii.

demonstrates that the simulation outcomes of the capillary bundle model devised in this study align well with the results obtained from laboratory experiments. In contrast to the uniform phase displacement, the relative permeability of the water phase in polymer particle dispersion system displacement is markedly reduced, whereas there is a notable increase in the oil phase's relative permeability. Furthermore, at higher water saturation levels, the relative permeability of the water phase in both scenarios exhibits a declining trend.

The initial distinction observed is a greater reduction in the water phase's relative permeability within the capillary bundle model presented in this study, attributed to

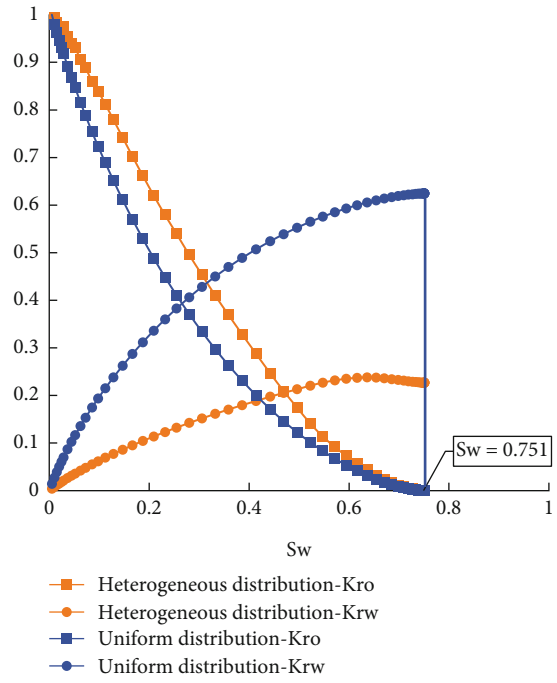

Figure 5: Relative permeability curve for displacement of homogeneous phase and polymer particle dispersion system.

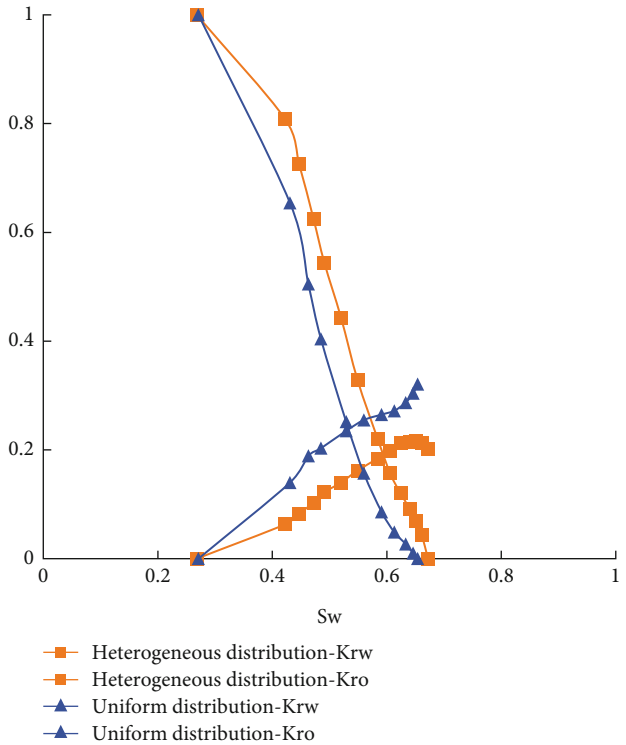

Figure 6: Relative permeability curve obtained from laboratory core displacement experiment [20].

differences in pore and capillary configurations between the two systems. The lack of pore distribution data from the referenced laboratory experiment means that a direct comparison of relative permeability curves cannot achieve perfect

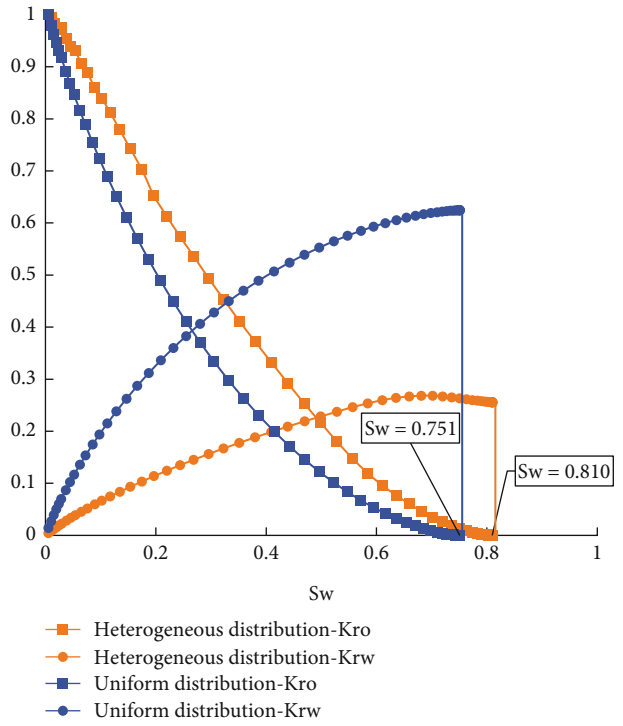

Figure 7: Relative permeability curve of polymer particle dispersion system under high displacement pressure.

alignment. Furthermore, the residual oil saturation indicated by the polymer particle dispersion system's relative permeability curve in experimental outcomes is lower compared to the homogeneous phase displacement. This discrepancy arises because both the homogeneous phase and polymer particle dispersion system were subjected to identical injection rates during the laboratory experiment, leading to a heightened displacement pressure gradient within the polymer particle dispersion system. Conversely, the capillary bundle model developed herein employs a consistent displacement pressure gradient for its calculations.

By enhancing the displacement pressure gradient in the capillary bundle model of the polymer particle dispersion system to 2 MPa, we derive the relative permeability curve illustrated in Figure 7. Notably, the residual oil saturation in the polymer particle dispersion system's relative permeability curve is reduced from 0.249 to 0.190, attributable to the boundary layer effect. As the displacement pressure gradient increases, the boundary layer's thickness diminishes, leading to a corresponding decrease in residual oil saturation.

When comparing these findings with laboratory core displacement experiment outcomes, the capillary bundle model, which accounts for the boundary layer effect in polymer particle dispersion systems for oil displacement, demonstrates significant precision.

4.2. Flow Characteristics of Polymer Particle Dispersion System. In order to facilitate the study of the flow characteristics and water control mechanism of polymer particle dispersion systems, the capillary bundle models used below all use the same displacement pressure.

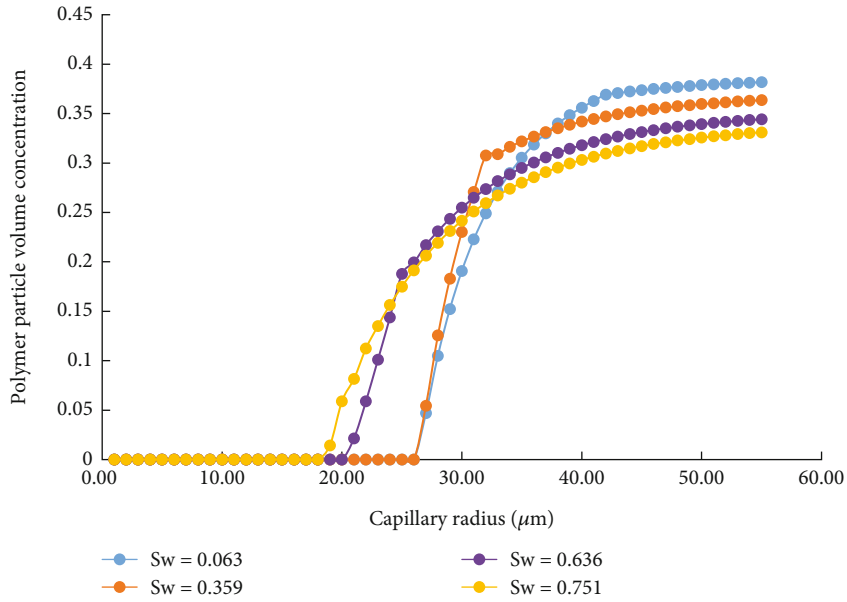

Figure 8: Volume concentration distribution of polymer particles in capillary at different water saturation.

Figure 5 facilitates the analysis of flow characteristics within polymer particle dispersion systems. A comparison of water phase relative permeability curves reveals a substantial decrease when polymer particles are distributed nonuniformly. This phenomenon occurs because capillary breakthrough leads to reduced flow resistance across the capillary, amplifying flow rates where breakthroughs have occurred. Consequently, the majority of particles migrate to these capillaries, elevating the system's viscosity and flow resistance. With rising water saturation, an increased number of capillaries are penetrated by the water phase, enhancing the water phase's flow resistance and amplifying the disparity in water phase relative permeability curves. At a water saturation of 0.656, the nonuniform distribution peaks the water phase relative permeability at 0.238. As water saturation climbs, this value declines, forming a concave curve in water phase relative permeability, culminating at a value of 0.227.

As delineated in Figure 5 through the analysis of oil phase relative permeability curves, a nonuniform distribution of polymer particles markedly enhances the oil phase's relative permeability. Prior to reaching a water saturation level of 0.3, there is a pronounced augmentation in the escalation in oil phase relative permeability correlating with an increase in water saturation. This augmentation is attributed to the segregation of the particle phase, which predominantly channels the polymer particles into larger capillaries that have been broken through by the water phase. Consequently, the dispersion system, characterized by its lower viscosity, predominantly flows to oil-saturated smaller and medium-sized capillaries, elevating the outlet flow rate of the oil phase. Beyond a water saturation level of 0.3, the escalation in oil phase relative permeability tapers off with further increases in water saturation. This trend is due to the water phase's continuous encroachment into larger and medium-sized capillaries, resulting in the oil phase's flow being predominantly restricted to smaller capillaries and a consequent reduction in the number of oil-saturated capillaries, which diminishes the oil phase's flow efficiency.

These observations lead to the conclusion that the heterogeneous distribution of polymer particles significantly inhibits the flow capacity of the dispersion system post-breakthrough. This effect facilitates greater displacement of the dispersion system into oil-saturated capillaries, thereby improving the oil phase's flow capacity.

4.3. Water Control Mechanism of Polymer Particle Dispersion System. By selecting various levels of water saturation and calculating the volumetric concentration of polymer particles within each capillary, we can analyze the water control mechanism operational within the polymer particle dispersion system. These calculations are detailed in Figure 8.

Analysis of Figure 8 reveals that at a water saturation of 0.063, polymer particles are predominantly concentrated in the broken large pore capillaries, with none entering capillaries smaller than 26 μm. As water saturation increases to 0.359, there is a notable decrease in polymer particle concentration in large pore capillaries, while those within the 26 μm to 36 μm range see a significant increase. With further increases in water saturation, the trend continues, with polymer particle concentration decreasing in larger pores and increasing in medium pores. At the peak water saturation of 0.751, capillaries smaller than 18 μm are devoid of polymer particles.

Drawing from the preceding analysis, the water control mechanism employed by the polymer particle dispersion system is elucidated. Initially, an abundant influx of polymer particles into the broken large pore capillaries heightens their flow resistance. This shift redirects the flow of fluids devoid of polymer particles into smaller and medium-sized pore capillaries that are richer in oil, thereby augmenting the oil phase's mobility. As the breakthrough process

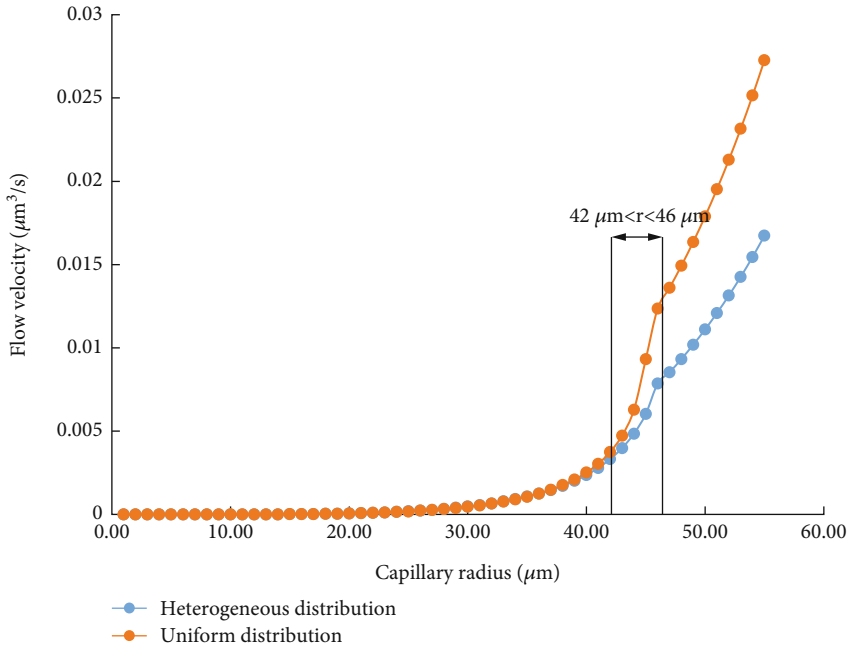

Figure 9: Comparison of liquid flow velocity in capillary between homogeneous phase and polymer particle dispersion system.

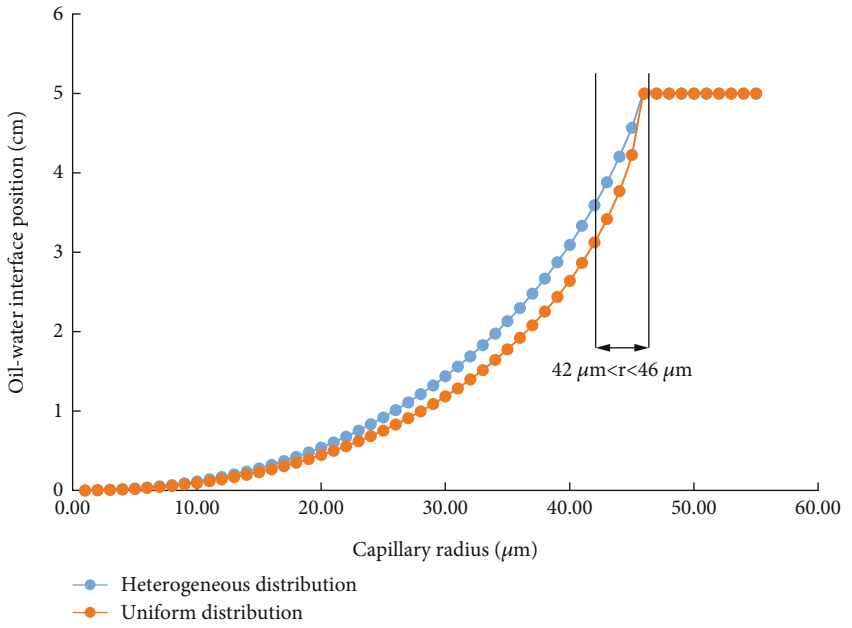

Figure 10: Comparison of oil-water interface positions in capillary between homogeneous phase and polymer particle dispersion system.

progresses into the smaller and medium-sized pore capillaries, polymer particles persist in infiltrating the now-penetrated larger and medium-sized pore capillaries. This action escalates the flow resistance across the water phase within the core, effectively managing water control. Concurrently, polymer particles spare the smaller oil-rich capillaries,

At a consistent water saturation level (Sw = 0.063), we calculated the fluid flow velocity and the position of the oil-water interface within each capillary for both the uniform and heterogeneous phases of polymer particles. This analysis highlights the water control benefits provided by the polymer particle dispersion system. The findings of these calculations are presented in Figures 9 and 10.

Reflecting on the polymer particle volume concentration distribution across capillaries at a water saturation of 0.063, as depicted in Figures 9 and 10, reveals that capillaries with pore diameters exceeding 46 μm have been penetrated. The considerable volume concentration of polymer particles within these capillaries accounts for the distinct flow velocities observed between the homogeneous and heterogeneous phases. While capillaries ranging from 42 μm to 46 μm have not yet been broken through, they feature larger oil-water

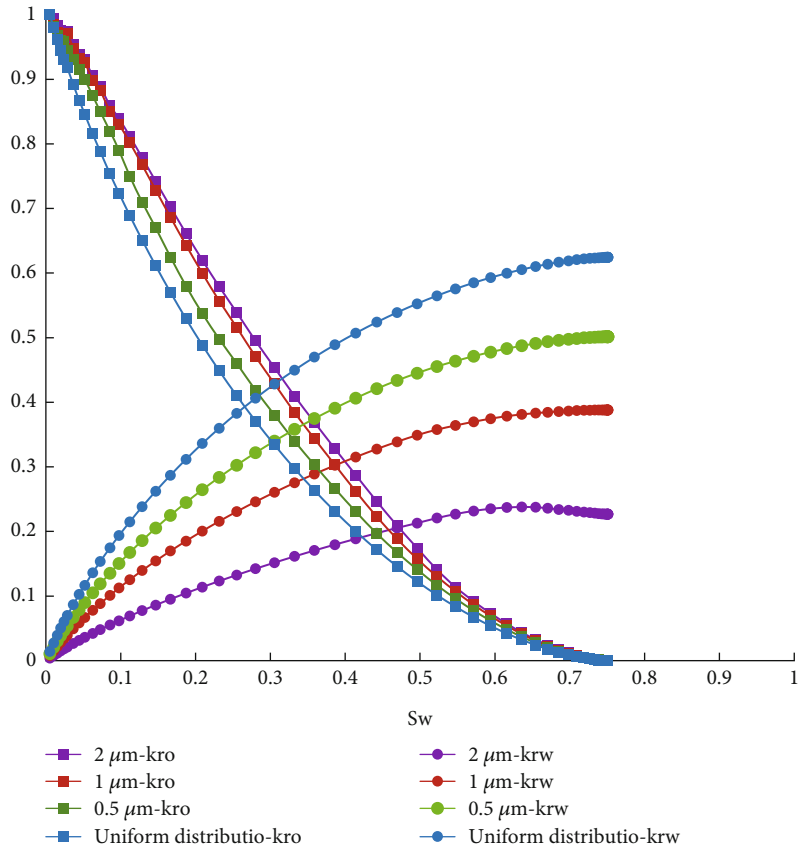

Figure 11: The effect of the initial particle size of different polymer particles on the relative permeability curve.

interface positions, minimal flow resistance, and a high polymer particle concentration, resulting in marked differences in fluid flow velocity between the two phases.

Under identical displacement pressure scenarios, the polymer particle dispersion system outperforms the homogeneous phase displacement by achieving more efficient oil extraction at reduced flow rates, demonstrating superior water control capabilities within broken capillaries.

4.4. Influence of the Initial Particle Size of the Polymer Particles. The impact of polymer particles' initial size on the oil displacement efficiency of the dispersion system was explored by adjusting the initial sizes to 2 μm, 1 μm, and 0.5 μm. According to Figure 11, a reduction in the polymer particles' size results in a relative permeability curve that increasingly resembles that of uniform phase displacement. This trend is attributed to the diminishing phase separation phenomenon and a more homogenous distribution of polymer particles during flow as their size decreases.

5. Conclusions

Relative to alternative simulation approaches, the oil displacement model for polymer particle dispersion systems developed herein adeptly delineates the effects of polymer particles' heterogeneous distribution within porous media. This offers pivotal technical insights for assessing the efficacy of oil displacement by polymer particle dispersion systems, marking a crucial advancement in the adoption and optimization of this technology. Further, alignment with laboratory core displacement experiments confirms the precision of our capillary bundle model, especially in its integration of boundary layer effects and polymer particles' heterogeneous distribution, in mirroring the actual flow characteristics encountered in polymer particle dispersion system displacement.

Simulation outcomes reveal that as water saturation escalates, the volume concentration of polymer particles in large pore capillaries diminishes, whereas it increases in medium pore capillaries. Upon reaching a peak water saturation of 0.751, capillaries smaller than 18 μm are devoid of polymer particles. This phenomenon suggests that the heterogeneous distribution of polymer particles plays a crucial role in mitigating the flow capacity of the dispersed system postwater phase breakthrough, thereby facilitating enhanced entry of the dispersion system into oil-rich capillaries and improving the oil phase's flow capacity.

Relative to uniform phase displacement, polymer particle dispersion systems exhibit superior oil recovery at lower flow rates in fractured capillaries, demonstrating more effective water control. Additionally, a reduction in polymer particle size leads to a decrease in phase separation, aligning the particles more closely with a uniform phase distribution during flow, which inversely affects their oil displacement efficiency.

Data Availability

The data used to support the findings of this study are available from the corresponding author upon request.

Conflicts of Interest

The authors declare that there are no conflicts of interest regarding the publication of this paper.

Acknowledgments

The authors wish to acknowledge the financial support from the National Natural Science Foundation of China (No. 51974343) and the Project of Sinopec Ministry of Science and Technology "Key Technology for Optimization Design of 3D Development of Shale Oil in Dongying Sag" (No. P23026).

References

[1] G. L. Lei and J. P. Zheng, "Synthesis of pore throat scale polymer microspheres and research on new technologies for full profile control and oil displacement," *Journal of China University of Petroleum*, vol. 3, no. 1, pp. 87–90, 2007.

[2] B. J. Bai, W. Liu, L. X. Li, G. H. Liu, and X. F. Tang, "Analysis of internal factors affecting the performance characteristics of pre-crosslinked gel particles," *Petroleum Exploration and Development*, vol. 29, no. 2, pp. 103–105, 2002.

[3] X. C. Wu, C. M. Xiong, H. B. Xu, and J. Zhang, "A novel particle-type polymer and IOR/EOR property evaluation," in *Abu Dhabi International Petroleum Exhibition and Conference*, Abu Dhabi, UAE, 2015.

[4] Z. Sun, X. G. Lu, and W. Sun, "The profile control and displacement mechanism of continuous and discontinuous phase flooding agent," *Journal of Dispersion Science and Technology*, vol. 38, no. 10, pp. 1403–1409, 2017.

[5] X. C. Chen, Q. H. Feng, W. Liu, and K. Sepehrnoori, "Modeling preformed particle gel surfactant combined flooding for enhanced oil recovery after polymer flooding," *Fuel*, vol. 194, pp. 42–49, 2017.

[6] H. Amedi and M. A. Ahmadi, "Experimental investigation the effect of nanoparticles on the oil-water relative permeability," *The European Physical Journal Plus*, vol. 131, no. 5, pp. 1–8, 2016.

[7] M. Yue, W. Y. Zhu, H. Y. Han, H. G. Song, Y. Q. Long, and Y. Lou, "Experimental research on remaining oil distribution and recovery performances after nano-micron polymer particles injection by direct visualization," *Fuel*, vol. 212, pp. 506–514, 2018.

[8] J. Wang, H. Q. Liu, Z. L. Wang, and C. H. Peng, "Experimental investigation on the filtering flow law of pre-gelled particle in porous media," *Transport in Porous Media*, vol. 94, no. 1, pp. 69–86, 2012.

[9] Q. H. Feng, X. C. Chen, and G. Zhang, "Experimental and numerical study of gel particles movement and deposition in porous media after polymer flooding," *Transport in Porous Media*, vol. 97, no. 1, pp. 67–85, 2013.

[10] A. Goudarzi, H. Zhang, A. Varavei et al., "A laboratory and simulation study of preformed particle gels for water conformance control," *Fuel*, vol. 140, pp. 502–513, 2015.

[11] X. Q. Liu, Z. Q. Qu, W. B. Ye et al., "A new type of double dispersion system for water control in fossil hydrogen energy development," *International Journal of Hydrogen Energy*, vol. 44, no. 56, pp. 29500–29507, 2019.

[12] M. L. Luo, X. H. Jia, X. D. Si, S. Luo, and Y. P. Zhan, "A novel polymer encapsulated silica nanoparticles for water control in development of fossil hydrogen energy—tight carbonate oil reservoir by acid fracturing," *International Journal of Hydrogen Energy*, vol. 46, no. 61, pp. 31191–31201, 2021.

[13] Z. Sun, X. C. Wu, X. D. Kang et al., "Comparison of oil displacement mechanisms and performances between continuous and dispersed phase flooding agents," *Petroleum Exploration and Development*, vol. 46, no. 1, pp. 121–129, 2019.

[14] Z. Xia, Y. Feng, and Z. H. Qian, "Study on factors affecting the sealing performance of polymer microsphere solutions," *Colloid and Polymer*, vol. 32, no. 1, pp. 38–40, 2014.

[15] Y. L. Zhou, H. Q. Jiang, C. Wang, G. Q. Sang, and L. Liu, "Research on micro percolation mechanism of polymer microsphere profile control and flooding by nuclear magnetic resonance," *Journal of Xi'an Shiyou University (Natural Science Edition)*, vol. 28, no. 1, pp. 70–75, 2013.

[16] M. Faivre, M. Abkarian, K. Bickraj, and H. A. Stone, "Geometrical focusing of cells in a microfluidic device: an approach to separate blood plasma," *Biorheology*, vol. 43, no. 2, pp. 147–159, 2006.

[17] A. R. Pries, K. Ley, M. Claassen, and P. Gaehtgens, "Red cell distribution at microvascular bifurcations," *Microvascular Research*, vol. 38, no. 1, pp. 81–101, 1989.

[18] S. M. McWhirter, R. Barbalat, K. M. Monroe et al., "A host type I interferon response is induced by cytosolic sensing of the bacterial second messenger cyclic-di-GMP," *The Journal of Experimental Medicine*, vol. 206, no. 9, pp. 1899–1911, 2009.

[19] B. M. Fenton, R. T. Carr, and G. R. Cokelet, "Nonuniform red cell distribution in 20 to 100 μm bifurcations," *Microvascular Research*, vol. 29, no. 1, pp. 103–126, 1985.

[20] Y. Q. Long, W. Y. Zhu, F. Q. Song, H. Q. Song, and M. Yue, "Theory of multiphase flow control in low permeability reservoir with nanometer and micro polymer particle dispersion system," *Journal of Central South University (Natural Science Edition)*, vol. 46, no. 5, pp. 1812–1819, 2015.

[21] I. M. Krieger and Y. J. Dougherty, "A mechanism for non-Newtonian flow in suspensions of rigid spheres," *Transactions of the Society of Rheology*, vol. 3, no. 1, pp. 137–152, 1959.

[22] H. B. Su, D. C. Wang, P. Zhang et al., "A new method to calculate the relative permeability of oil and water in tight oil reservoirs by considering the nonlinear flow," *Geofluids*, vol. 2022, Article ID 9450967, 14 pages, 2022.

[23] X. L. Li and J. Y. He, "Research and application of radial borehole fracturing based on numerical simulation," *Geofluids*, vol. 2019, Article ID 2167094, 16 pages, 2019.

[24] F. Civan and E. C. Donaldson, "Relative permeability from unsteady-state displacements with capillary pressure included," *SPE Formation Evaluation*, vol. 4, no. 2, pp. 189–193, 1989.

[25] C. Z. Cui, Y. F. Sui, X. Z. Cheng, Y. Z. Ye, and Z. Wang, "Numerical simulation of low-permeability reservoirs with considering the dynamic boundary layer effect," *Geofluids*, vol. 2021, Article ID 6637727, 8 pages, 2021.

[26] X. F. Tian, L. S. Cheng, Y. Q. Yan, H. J. Liu, W. Q. Zhao, and Q. Guo, "An improved solution to estimate relative permeability in tight oil reservoirs," *Journal of Petroleum Exploration and Production Technology*, vol. 5, no. 3, pp. 305–314, 2015.